

## Multifunctional properties of electrodeposited nickel composite coating containing nanosized monoclinic zirconia particles

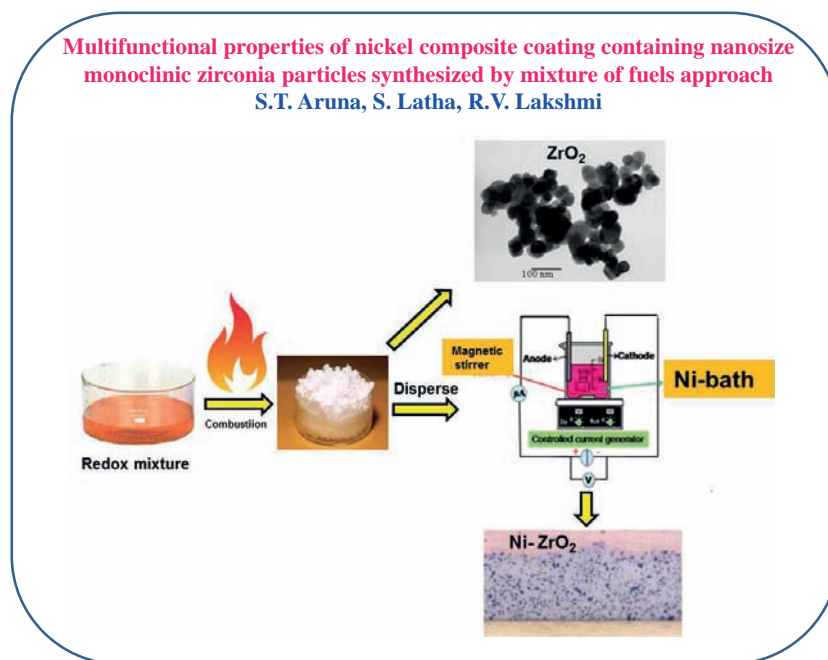
S.T. ARUNA\*, S. LATHA and R.V. LAKSHMI

Surface Engineering Division, Council of Scientific and Industrial Research-National Aerospace Laboratories, HAL Airport Road, Bangalore 560017, India

**Abstract :** Nickel-based composite coatings containing ceramic particles as the distributed phase have been widely used in aerospace and automotive industries. In the present work, a Ni-composite coating containing nanosized monoclinic zirconia ( $ZrO_2$ ) powder is prepared by solution combustion (SC) method. The SC method is modified to get phase pure white zirconia powder by using the mixture of fuels approach. Since the synthesized powder contained agglomerated particles, the powder is ball milled and dispersed in a nickel sulphamate bath. The Ni and Ni- $ZrO_2$  coatings are electrodeposited at  $0.75 \text{ A/dm}^2$  for 6 h. The Ni- $ZrO_2$  composite coating exhibits a microhardness of 750 KHN(50 gf) as against 270 KHN(50 gF) observed for plain Ni coating. The Ni- $ZrO_2$  coating exhibits improved corrosion resistance and wear resistance compared to plain nickel coating as confirmed by potentiodynamic polarization and continuous salt spray tests. The as-deposited hydrophobic Ni- $ZrO_2$  coating transforms to superhydrophobic upon depositing a thin layer of fluoroalkyl silane on the coating. Thus, the synthesized zirconia particles when incorporated in the Ni matrix impart multifunctional properties to the electrodeposited Ni coating.

**Keywords:** Electrodeposited; composites; nickel; zirconia; corrosion; wear; superhydrophobic

### Graphical Abstract



### INTRODUCTION

Nickel-based composites containing reinforced particles are playing a pivotal role in aerospace and automotive industries owing to their high specific strength, excellent mechanical properties, good thermal stability, good toughness, chemical inertness, high wear resistance and corrosion resistance<sup>[1]</sup>. Silicon carbide has been the most widely used reinforcement mainly owing to its high hardness and higher wear resistance<sup>[2-4]</sup>. Further, to extend the application of electrodeposited Ni composite coatings for higher temperatures, oxide

\* Corresponding Author Email: aruna\_reddy@nal.res.in

particles have been explored in lieu of SiC particles. The important reinforcement or distributive phases that have been explored in the literature are  $\text{Al}_2\text{O}_3$  [5],  $\text{TiO}_2$  [6],  $\text{Fe}_2\text{O}_3$  [7],  $\text{CeO}_2$  [8],  $\text{ZrO}_2$  [9], diamond [10], graphite [11], carbon nanotubes (CNTs) [12], etc. The research arena of electrodeposited composite coatings continues to expand. More recent papers are focused towards utilizing graphene/graphene oxide [13-19] and a mixture of phases [20] as distributive phases in Ni matrix. There has been renewed interest in using non-oxide ceramics such as TiC and TiN as fillers in electrodeposited Ni composite coatings on tungsten carbide cutting tools [21]. Among the different distributed phases studied, zirconia is an important ceramic material as it is known for its excellent high temperature mechanical properties, thermal shock resistance, wear and oxidation resistance, low thermal conductivity and reasonable match in thermal expansion coefficient to that of metals [22]. Pure  $\text{ZrO}_2$  has a monoclinic crystal structure at room temperature and undergoes transitions to tetragonal and cubic phases at increasing temperatures. It is observed that in most of the reported Ni- $\text{ZrO}_2$  composite coatings [23-27] commercially available zirconia powder is being used and seldom the phase of zirconia is mentioned. A recent publication shows the prospects of using Ni- $\text{ZrO}_2$  nanocomposite on the surface of the copper plate of crystallizer, an important equipment used for continuous casting production at  $280^\circ\text{C}$  [28].

In the present study, electrodeposited Ni composite coating containing monoclinic zirconia as the distributive phase exhibiting multifunctional properties is described. The monoclinic zirconia powder has been prepared by solution combustion technique. The process has been modified to get phase pure, carbon free monoclinic zirconia powder. The powder has been characterized for phase purity and morphology. The synthesized powder has been used as the filler in electrodeposited Ni composite coating. The obtained coating has been characterized for microstructure, phase, mechanical, and wear and corrosion properties. The wettability of the coatings has also been studied.

## EXPERIMENTAL

### *Preparation and characterization of $\text{ZrO}_2$ powder*

Solution combustion method, which is one of the most popular methods for the synthesis of nanosize oxides, has been utilized for the synthesis of zirconia powder [29]. For the preparation of phase pure and carbon free white zirconia powder, the redox mixture composition used for solution combustion was optimized (Table-1). The temperatures measured during solution combustion synthesis using a K-type thermocouple are also tabulated in Table-1. Phase pure white zirconia powder was prepared by a mixture of fuels approach as follows: 0.031 M of  $\text{ZrOCl}_2$  was dissolved in water to which 10 mL of nitric acid was added and stirred well. To the clear solution, 62.06 g urea, 21.72 g ammonium acetate and 37.5 g ammonium nitrate were added. The clear solution was transferred to alumina crucible and placed in a furnace pre-heated to  $350^\circ\text{C}$ . The solution boils, froths, catches fire and gives voluminous white oxide powder. It was found that a combination of mixture of fuels and oxidizers facilitated the formation of pure white zirconia particles devoid of carbon traces and which may be attributed to the higher flame temperature observed with this composition.

**Table-1. Solution combustion synthesis parameters used for the preparation of monoclinic zirconia powder.**

S. No.	Mole ratio of Oxidizers		Mole ratios of Fuels			Flame temp. ( $^\circ\text{C}$ )	Nature of combustion	Powder color
	$\text{ZrOCl}_2 \cdot 8\text{H}_2\text{O}$	$\text{NH}_4\text{NO}_3$	Glycine	Urea	Ammonium acetate			
1	0.031	---	0.069	---	---	238	Flameless	Black
2	0.031	---	0.034	0.052	0.028	317	Flameless	Black
3	0.031	---	0.035	0.052	0.056	330	Flameless	Black

S. No.	Mole ratio of Oxidizers		Mole ratios of Fuels			Flame temp. (°C)	Nature of combustion	Powder color
	ZrOCl <sub>2</sub> ·8H <sub>2</sub> O	NH <sub>4</sub> NO <sub>3</sub>	Glycine	Urea	Ammonium acetate			
4	0.031	---	0.017	0.077	0.028	325	Flameless	Black
5	0.031	0.012	---	0.103	0.028	330	Flameless	Dull white
6	0.031	0.025	---	0.103	0.028	350	Flameless	Dull White
7	0.031	0.025	---	0.103	0.028	400	Dull flame with orange sparks	Dull White
8	0.031	0.031	---	0.103	0.028	450	Flame with orange sparks	White
9	0.031	0.047	---	0.103	0.028	700	Bright flame	Pure white

The phase purity and crystallite size of the synthesized powder was determined using a powder X-Ray diffractometer (Bruker D8 Advance, CuK $\alpha$  radiation). The monoclinic phase present in the synthesized zirconia powder was identified from XRD pattern using JCPDS card: 37-1484. The morphology of the synthesized zirconia powder was obtained by Field Emission Scanning Electron Microscope (FESEM, Carl Zeiss). The particle size distribution of the powders was measured using a particle size analyzer (Mastersizer 2000, Malvern instruments). The transmission electron micrograph (TEM) of the zirconia particle was measured using JEOL-JEM 100SX transmission electron microscope.

#### *Development of electrodeposited Ni-ZrO<sub>2</sub> composite coating*

Nickel sulfamate plating bath with the composition as detailed in Table-2 was used for depositing Ni and Ni-ZrO<sub>2</sub> coatings. About 200 mL of Ni-sulfamate plating bath containing 20 g of synthesized ZrO<sub>2</sub> particles was taken in a glass beaker and its pH was adjusted to 4. A pure nickel sheet with a dimension of 2.5 cm x 12 cm was used as anode and a polished brass substrate with similar dimension as the anode was employed as cathode. The brass substrate was degreased with acetone and cathodically cleaned by dipping it in a mild alkali (20% NaOH) at 0.0645A/dm<sup>2</sup> and dipped in 10% H<sub>2</sub>SO<sub>4</sub>. It was finally washed with distilled water. The above electrolyte bath containing zirconia particles was magnetically stirred with ~600 rpm for 15 hours before the deposition and during co-deposition to confirm proper dispersion of particles in the bath. The co-deposition was carried out on the brass substrate area of 2.5 cm x 3.75 cm using a current density of 0.75 A/dm<sup>2</sup> for a duration of 6 h to obtain a deposit thickness of ~ 40  $\mu$ m according to Faraday's laws. These parameters were chosen based on the optimized parameters of the previous study<sup>[30]</sup>.

**Table-2. Composition of the nickel sulfamate bath used for electrodeposition.**

S. No.	Plating bath chemicals	Supplier	Composition
1.	Nickel sulfamate solution (50 g Ni/L)	Grauer & Weil, India	300 g/L
2.	Nickel chloride	S.D Fine	10 g/L
3.	Boric acid	S.D Fine	30 g/L
4.	Sodium lauryl sulfate	S.D Fine	0.2 g/L
5.	Zirconia powder	In-house synthesized	100 g/L

**Characterization of developed Ni-ZrO<sub>2</sub> composite coating**

**Phase, microstructure, surface roughness and microhardness of Ni and Ni-ZrO<sub>2</sub> composite coatings**

The XRD patterns were indexed as per the JCPDS no. 4-850. The relative texture coefficients (RTC(hkl)) were calculated for electrodeposited Ni and Ni-ZrO<sub>2</sub> composite coatings based on their XRD patterns<sup>[31]</sup>. The texture and preferred orientation of Ni and Ni-ZrO<sub>2</sub> films was calculated by employing relative texture coefficient RTC<sub>hkl</sub> (eqn. 1):

$$RTC_{hkl} = \frac{I_{hkl} / I_{hkl}^0}{\sum_1^3 I_{hkl} / I_{hkl}^0} \cdot 100\% \quad \dots\dots\dots (1).$$

where Ihkl are the relative intensities of the (hkl) reflections, Σ I<sub>hkl</sub> is the sum of all the peak intensities corresponding to (111), (200), and (220) peaks of Ni. In the equation I<sub>hkl</sub><sup>0</sup> refers to the relative intensities of a randomly oriented nickel powder sample.

The surface microstructure of as deposited coatings was observed using FESEM. The surface roughness of the coatings was also analyzed using 3D-profilometer (Nanomap 500LS, AEP Technology)

To prepare, the samples for cross-sectional imaging and microhardness determination the as-deposited Ni and Ni-ZrO<sub>2</sub> coatings were coated with Cu backup layer. Then the coating along with the substrate was cut and mounted in a Bakelite matrix. Then the samples were ground with various grades of emery followed by metallographic polishing (down to 0.05 μm) using alumina slurry. The Knoop microhardness was measured on the cross-section at ten different locations using a load of 50 gF (Micromet 2103, Buehler). The microstructure of the cross section of Ni-ZrO<sub>2</sub> coating was recorded using a microscope.

**Corrosion studies**

The corrosion studies of Ni and Ni-ZrO<sub>2</sub> coatings on brass substrates were conducted in deaerated 3.5 wt% (0.6 M) NaCl solution (200 ±2 ml) using an electrochemical workstation (CHI 604 2D). The test was conducted using Ni and Ni-ZrO<sub>2</sub> coated brass coupons with an active area of 1cm<sup>2</sup> each as working electrodes, platinum foil as counter electrode and a standard saturated Calomel electrode as the reference electrode. The details of potentiodynamic polarization have been already reported<sup>[32]</sup>. The corrosion potential (E<sub>corr</sub>), corrosion current density (i<sub>corr</sub>) and polarization resistance (Rp) were deduced from the Tafel plot and are summarized in Table-3. The polarization resistance was obtained using the Stern-Geary equation<sup>[33]</sup>.

$$R_p = \left[ \frac{b_a b_c}{2.303(b_a + b_c)} \right] \left[ \frac{1}{i_{corr}} \right] \quad \dots\dots\dots 2$$

Where b<sub>a</sub> and b<sub>c</sub> are Tafel slopes or the Tafel constants, expressed in mV/dec.

Corrosion rates (CR) were calculated by the following equation:

$$CR = \frac{1.13 i_{corr} \times Eq. \text{ wt. of Ni}}{\text{Density of Ni}} \quad \dots\dots\dots 3$$

The samples were also subjected to accelerated corrosion by placing them in a highly corrosive conditions (5% NaCl solution) in a continuous salt spray chamber (Ascott Sxp 120,) as per ASTM B117 standard. The coatings were also tested for 2400 h.

**Table-3 : Relative texture coefficients of Ni and Ni-ZrO<sub>2</sub> electrodeposited coatings.**

Sample	Relative Texture Coefficient (%)		
	(111)	(200)	(220)
Ni	15.54	56.35	28.09
Ni-ZrO <sub>2</sub>	39.84	33.30	26.84

### ***Wear studies***

The wear resistance of the electrodeposited Ni and Ni-ZrO<sub>2</sub> composite coatings on brass pin (radius 6 mm) was investigated using a pin-on-disk wear tester (DUCOM, India) under ambient conditions of temperature and humidity (30°C, 50% RH) at an applied load of 9.8 N. The counterpart was hardened EN31 steel disk with a hardness of 750 HV. Complete details regarding the wear studies have already been reported [32]. The wear coefficient was calculated using the Holm-Archard relationship [34, 35].

### ***Water repellent property of Ni and Ni-ZrO<sub>2</sub> composite coatings***

The brass substrates coated with Ni and Ni-ZrO<sub>2</sub> coatings were surface modified with a low surface energy material like 1 wt% of fluoro alkyl silane (FAS-17, ABCR GmbH) ethanolic solution using a paint spray gun. The FAS treated coatings were dried at 80 °C for 1 h. The water contact angles (WCA) on the surface of as-deposited and FAS treated Ni and Ni-ZrO<sub>2</sub> coatings were measured at room temperature using a contact angle meter (Surface Electro Optics, Phoenix) by sessile drop method by placing 8 µL water drops on the surface of the coatings. The average value of five WCA measurements at different positions of each coating is reported as the final WCA.

## **RESULTS AND DISCUSSION**

### ***Powder characterization***

Figure 1 shows the XRD pattern of as calcined ZrO<sub>2</sub> powder. The XRD peaks correspond to monoclinic zirconia phase and peaks corresponding to either tetragonal or cubic phases of zirconia were not observed. The crystallite size as calculated from Scherrer equation was 26 nm.

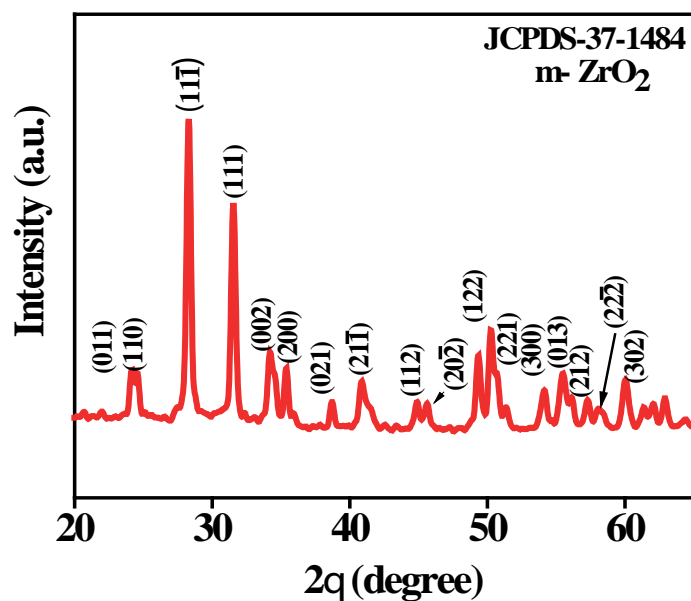


*Fig. 1. Powder XRD pattern of solution combustion synthesized zirconia powder.*

The particle size distribution curve of zirconia powder (Fig. 2) exhibits a uniform distribution of particles. The average agglomerated particle size was 2.875  $\mu\text{m}$  with 90% of the particles below 9.5  $\mu\text{m}$  and 10% of the particles below 0.876  $\mu\text{m}$ .

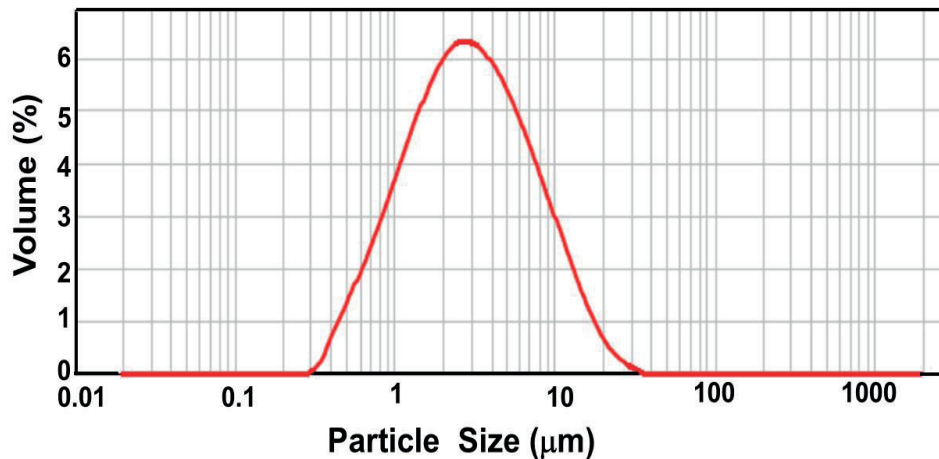


Fig. 2. Particle size distribution of ball-milled  $\text{ZrO}_2$  powder.

The FESEM image of as prepared zirconia powder showed flaky structure (not shown). The FESEM images of ball-milled zirconia powder is shown in Fig.3a. The FESEM image of zirconia powder exhibited smaller agglomerated particles. The particle size seems to vary from 50-100 nm with some bigger agglomerated particles. The TEM image clearly shows distinct particles with the majority of the particles having < 50 nm size (Fig.3b).

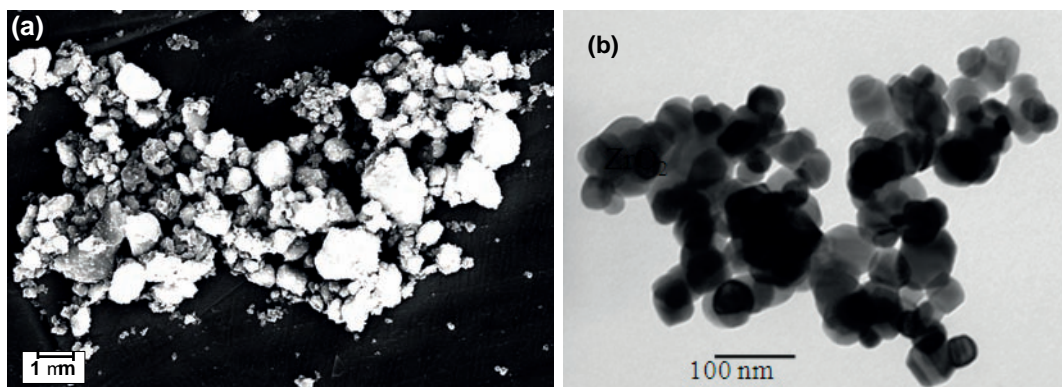


Fig. 3. (a) FESEM and (b) TEM images of ball milled  $\text{ZrO}_2$  powder.

#### *Phase, microhardness, microstructure and surface roughness of Ni and Ni-ZrO<sub>2</sub> coatings*

Figure 4 shows the XRD patterns of electrodeposited Ni and Ni-ZrO<sub>2</sub> coatings. It is evident from the XRD patterns that pure nickel coating exhibited intense peaks at 44° and 51° corresponding to Ni (111) and (200) planes respectively. The XRD pattern of Ni-ZrO<sub>2</sub> composite coating showed ZrO<sub>2</sub> peak which clearly indicates the incorporation of large number of particles in the coating.

There was also a slight change in the relative texture coefficients for Ni and Ni-ZrO<sub>2</sub> composite coatings (Table-III). The preferred orientation through an axis [hkl] was selected by values of RTC  $\geq 25\%$  such that when the RTC approaches the value of 100%, the strength of the preferred orientation becomes maximum amount. The (200) peak intensity was highest for Ni and for Ni-ZrO<sub>2</sub> the peak intensity was highest for (111). The preferred orientation in Ni was [200] and in case of Ni-ZrO<sub>2</sub>, [111] was the preferred orientation.

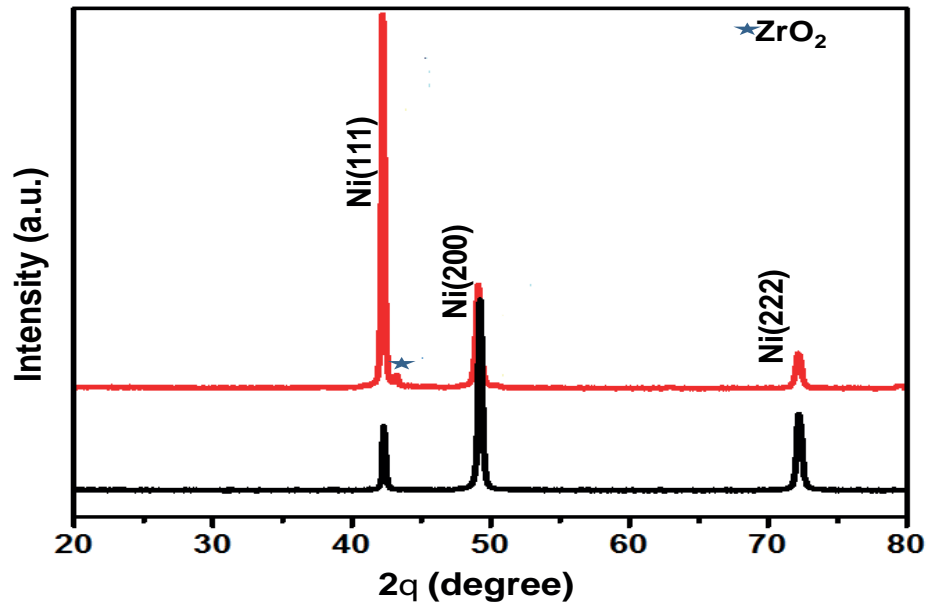


Fig. 4. XRD patterns of electrodeposited (a) Ni and (b) Ni-ZrO<sub>2</sub> composite coatings.

The Ni crystallite sizes as calculated from Scherrer formula were 32 and 24 nm for Ni and for Ni-ZrO<sub>2</sub> it was 38 and 19 nm respectively for the peaks corresponding to (111) and (200) respectively. From this, it is evident that there is not much of a change in the crystallite size of nickel with the incorporation of zirconia particles. The optical micrograph of Ni-ZrO<sub>2</sub> coating is shown in Fig. 5. It shows a uniform distribution of particles. The presence of agglomerated particles is also evident.

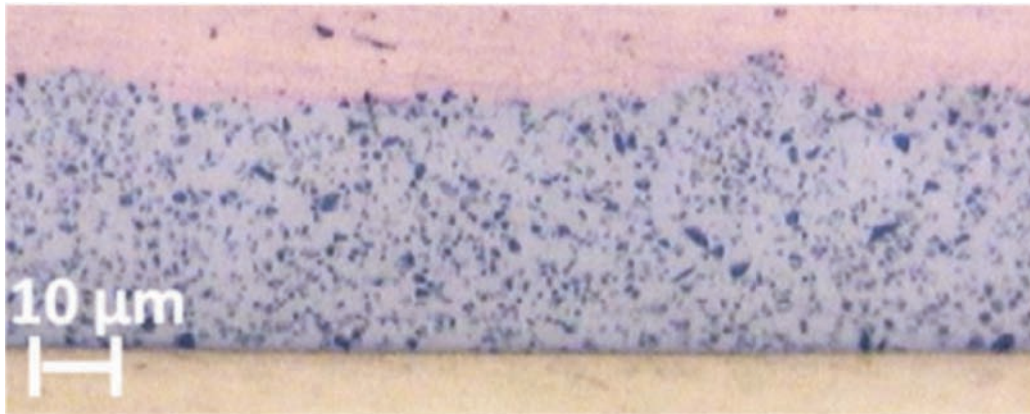


Fig. 5. Optical micrograph of Ni-ZrO<sub>2</sub> coating electrodeposited at 0.75 A/dm<sup>2</sup>.

The Ni-ZrO<sub>2</sub> composite coating exhibited a microhardness of 750±10 KHN (50 gf) and Ni electrodeposited under similar conditions exhibited a microhardness of 270±10 KHN(50 gf). Since the grain refinement was not remarkable in case of Ni-ZrO<sub>2</sub>, the dispersive strengthening effects would have dominated resulting in higher microhardness of the composite. Thus the enhancement of microhardness of Ni-ZrO<sub>2</sub> composite coating can also be related to the dispersion-strengthening effect caused by ZrO<sub>2</sub> particles in the composite coatings, which obstruct the motion of dislocations in the Ni matrix<sup>[36]</sup>.

Figure 6 shows the surface topography of Ni and Ni-ZrO<sub>2</sub> composite coating. Ni coating shows more uniform surface and Ni-ZrO<sub>2</sub> coating shows the presence of some protrusions clearly indicating a rough surface. The surface roughness was 628 and 193 nm respectively for Ni-ZrO<sub>2</sub> and Ni coatings.

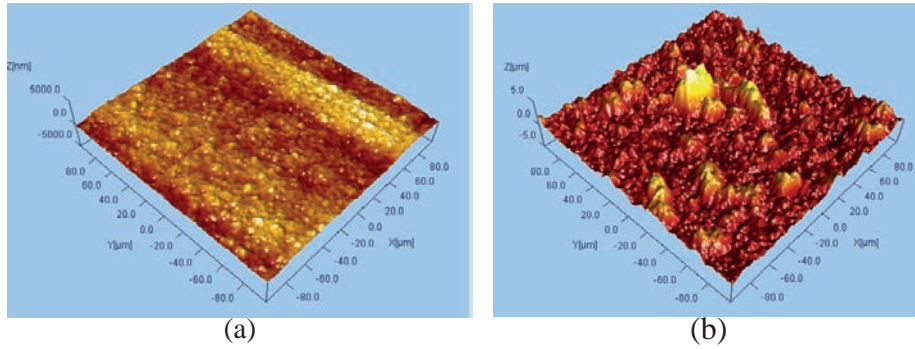


Fig. 6. 3D-image showing the surface roughness and topography of electrodeposited (a) Ni and (b) Ni-ZrO<sub>2</sub> coatings.

The pure nickel deposit exhibited a rather regular surface (not shown), whereas the composite coating developed an uneven surface containing nodular features (Fig.7). The zirconium oxide particles are clearly seen on the surface. Also, white zirconia particles are homogeneously distributed on the surface.

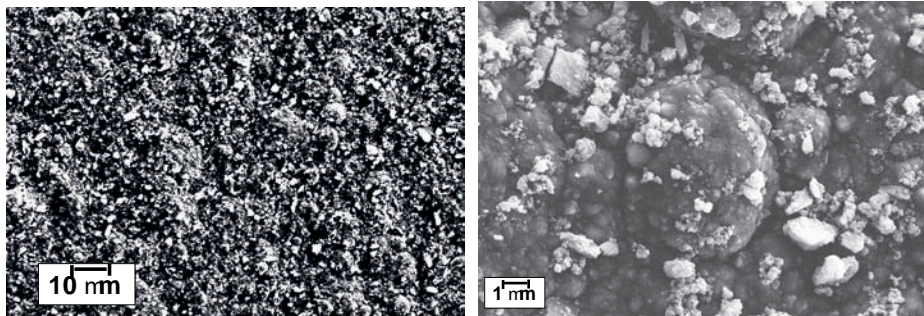


Fig. 7. FESEM image of electrodeposited Ni-ZrO<sub>2</sub> composite coating at two different magnifications.

The X-ray mapping images of Ni, Zr and O elements present in Ni-ZrO<sub>2</sub> composite coating are shown in Fig.8. The X-ray mapping clearly shows incorporation of a large fraction of zirconia particles in the Ni-ZrO<sub>2</sub> coating. The average EDAX data recorded on various spots of Ni-ZrO<sub>2</sub> coating surface (Fig.8) are tabulated in Table-4. The EDAX results indicate a higher wt% of ZrO<sub>2</sub> incorporation.

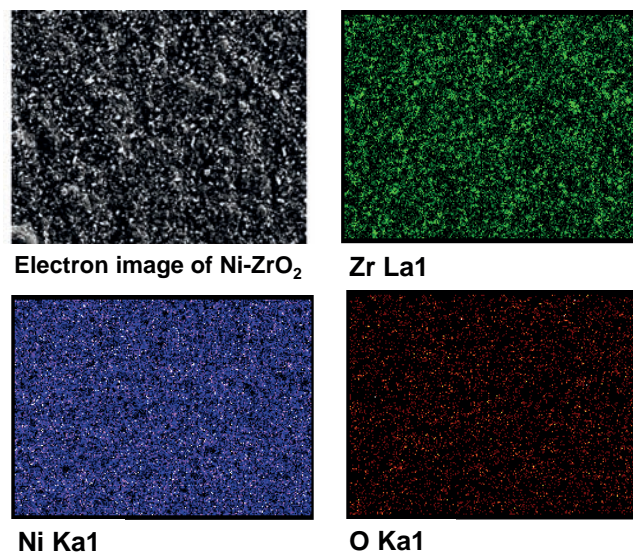


Fig. 8. Electron image of Ni-ZrO<sub>2</sub> coating and X-ray mapping images of Ni, Zr and O elements present in Ni-ZrO<sub>2</sub> coating.

**Table-4 : EDAX results taken on Ni-ZrO<sub>2</sub> coating surface.**

Element	Weight %
O	4.73
Zr	16.93
Ni	78.35
Total	100.00

**Potentiodynamic polarization and EIS studies**

The Tafel plots corresponding to Ni and Ni-ZrO<sub>2</sub> composite coatings are shown in Fig. 9 and the obtained polarization parameters are listed in Table-5. When compared to plain nickel coating, the corrosion potential of the Ni-ZrO<sub>2</sub> coating moved towards more positive side, suggesting enhanced corrosion resistance of the coating. The corrosion current density (*i*<sub>corr</sub>) is a crucial parameter which indicates the kinetics of the corrosion reaction. Lower the corrosion current density value, higher will be the corrosion protection. The corrosion current density value for the Ni-ZrO<sub>2</sub> coating was very low (0.161 μA/cm<sup>2</sup>) compared to plain Ni (28.65 μA/cm<sup>2</sup>) indicating improved corrosion resistance of the Ni-ZrO<sub>2</sub> coating. This observation was further substantiated by the observed higher polarization resistance (*R*<sub>p</sub>) value (189 kΩ cm<sup>2</sup>) for Ni-ZrO<sub>2</sub> coating.

**Table-5 : Potentiodynamic polarization results of Ni and Ni-ZrO<sub>2</sub> composite coatings.**

Sample	OCP(V) vs. SCE	E <sub>corr</sub> (V) vs. SCE	<i>i</i> <sub>corr</sub> (μA/cm <sup>2</sup> )	<i>R</i> <sub>p</sub> (kΩ cm <sup>2</sup> )	<i>b</i> <sub>a</sub> (V/dec)	<i>b</i> <sub>c</sub> (V/dec)	Corrosion rate (g/h)
Ni	-0.482	-0.471	28.65	1.44	0.157	0.2375	1.07x10 <sup>-4</sup>
Ni-ZrO <sub>2</sub>	-0.105	-0.107	0.16	189	0.163	0.1239	6.02x10 <sup>-7</sup>

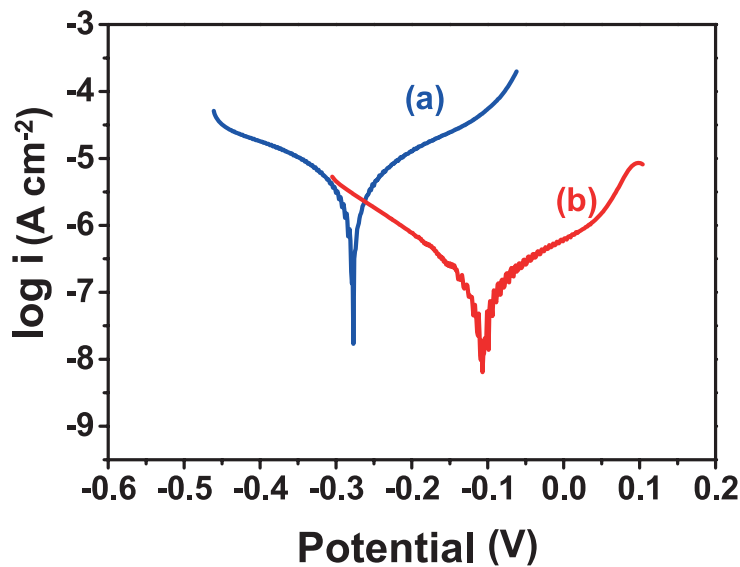


**Fig. 9. Tafel plots of electrodeposited (a) Ni and (b) Ni-ZrO<sub>2</sub> coatings.**

Plain brass substrate and Ni-ZrO<sub>2</sub> coated substrates were subjected to continuous salt spray test for 168 h and prolonged 2400 h salt spray. There were no corrosion products on the Ni-ZrO<sub>2</sub> surface. The Ni-ZrO<sub>2</sub> coating was intact even after 2400 h of salt spray test. There were no visible changes on the surface of the Ni-ZrO<sub>2</sub> coating which indicates better corrosion resistance of the coating. This has been already confirmed by potentiodynamic polarization study.

### *Wear resistant property of Ni-ZrO<sub>2</sub> coatings*

The wear data of Ni and Ni-ZrO<sub>2</sub> composite coatings are summarized in Table-6. It can be observed from the table that Ni-ZrO<sub>2</sub> coating is exhibiting better wear resistance (lower wear loss). It is also gratifying to note that Ni-ZrO<sub>2</sub> composite coating shows lower coefficient of friction and lowest wear rate compared to plain nickel. The lower wear rate can be attributed to the higher and uniform incorporation of zirconia particles in the nickel matrix. The higher fracture toughness of monoclinic zirconia particles could have also resulted in improved wear resistance as the wear resistance of zirconia increases with the fourth power of its fracture toughness<sup>[37]</sup>.

**Table-6. Comparative wear properties of Ni and Ni-ZrO<sub>2</sub> coatings.**

Coating	Average coefficient of friction	Wear loss (µm)	Wear volume loss(mm <sup>3</sup> )	Wear coefficient	Wear rate (mm <sup>3</sup> /Nm)
Pure Ni	0.789	90	0.12647	1.39x10 <sup>-8</sup>	5.59x10 <sup>-5</sup>
Ni-ZrO <sub>2</sub>	0.515	14	0.00307	8.67x10 <sup>-10</sup>	1.36x10 <sup>-9</sup>

### *Superhydrophobic property of Ni and Ni-ZrO<sub>2</sub> coatings*

In the present study, the WCA of as deposited and FAS treated Ni and Ni-ZrO<sub>2</sub> surfaces were measured and are shown as histogram (Fig.10). Although there was not much variation in the WCA of as-deposited Ni (89°) and Ni-ZrO<sub>2</sub> (95°) coatings, there was a drastic rise in the WCA of FAS treated Ni-ZrO<sub>2</sub> coating. Ni-ZrO<sub>2</sub> coating exhibited superhydrophobic property with a WCA~157° and Ni showed hydrophobic property with a WCA~109°. The higher WCA observed in Ni-ZrO<sub>2</sub> coating may be attributed to its higher surface roughness (628nm) consisting of hierarchical micro and nano roughness due to the combination of matrix and zirconia particle roughness. The formed coating contains trapped air pockets leading to Cassie Baxter state resulting in superhydrophobicity. The obtained WCA value is higher than that reported in the literature for Ni-TiO<sub>2</sub> (140°) surface treated with trimethoxy(propyl)silane solution<sup>[6]</sup>.

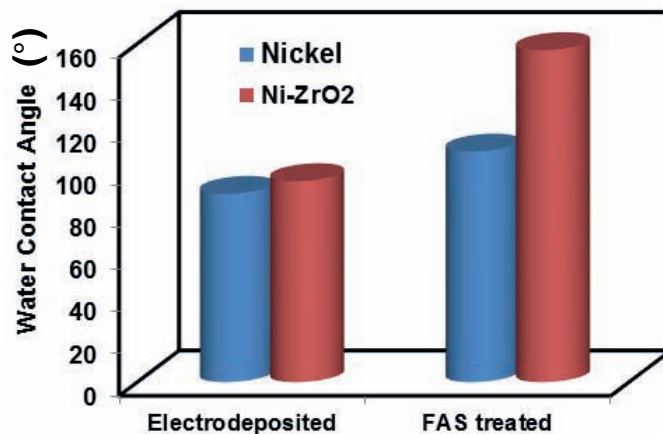


**Fig.10. Histogram showing the water contact angle of as deposited and FAS treated Ni and Ni-ZrO<sub>2</sub> electrodeposited coatings.**

## CONCLUSIONS

In the present study, electrodeposited Ni-ZrO<sub>2</sub> coating exhibiting multi-functional properties was developed. Nanosized monoclinic zirconia powder was prepared by solution combustion method using a mixture of fuels and extra oxidizer. The obtained powder was subjected to ball-milling before electrodeposition to reduce the agglomeration of the particles. The coating electrodeposited at 0.75 A/dm<sup>2</sup> was used for corrosion and wear studies. The Ni-ZrO<sub>2</sub> coating exhibited improved corrosion and wear resistance compared to plain Ni coating. The Ni-ZrO<sub>2</sub> coatings also exhibited a lower coefficient of friction and lower wear loss compared to plain Ni

coating. The Ni-ZrO<sub>2</sub> coating also exhibited a higher water contact angle and can find potential use in applications requiring hydrophobic property. Thus, the developed Ni-ZrO<sub>2</sub> is a multi-functional coating exhibiting a synergistic combination of higher microhardness, improved wear resistance and corrosion resistance and superhydrophobic property.

## ACKNOWLEDGMENTS

The authors thank Director and Head, SED, CSIR- NAL for their constant encouragement. The authors also thank Mujibir, A. Sreenivasan, Muni Prakash, Siju, and Dinesh for the help received in electrodeposition, corrosion testing, wear testing, FESEM, microhardness and contact angle measurement studies respectively. The author thanks Dr. Shay Tirosh from Bar-Ilan University for the TEM study.

## REFERENCES

- [1] F.C. Walsh, S. Wang, N. Zhou: The electrodeposition of composite coatings: Diversity, application and challenges. *Curr Opin Electrochem*, 20: 8-19, 2020.
- [2] L. Ghelani, M. Naoun, L. Aissani, A. Abbassi, S. Boulahrouz: Electrodeposition and mechanical characterization of Ni/SiC composite coatings, *J. Nano- and Electron Phys* 11 (3): 03016, 2019.
- [3] G. Gyawali, K. Hamal, B. Joshi, A. Rajbhandari, S. Wohn Lee: Microstructural and electrochemical analysis of Ni-SiC composite coatings prepared in presence of additives, *Mater Lett* 126: 228-231, 2014.
- [4] S.T. Aruna, C. Anandan, V.K.W. Grips: Effect of probe sonication and sodium hexametaphosphate on the microhardness and wear behavior of electrodeposited Ni-SiC composite coating, *Appl Surf Sci* 301: 383-390, 2014.
- [5] O. Yilmaz, M. Erdogan, I. Karakaya: Combined effects of ALS and SLS on Al<sub>2</sub>O<sub>3</sub> reinforced composite nickel coatings, *Surf Eng* 36 (5): 477-484, 2020.
- [6] M. Salehi, M. Mozammel, S.M. Emarati: Superhydrophobic and corrosion resistant properties of electrodeposited Ni-TiO<sub>2</sub>/TMPSi nanocomposite coating, *Colloids Surf A: Physicochem Eng Asp* 573: 196-204, 2019.
- [7] I.U. Haq, K. Akhtar, T.I. Khan, A. Ali Shah: Electrodeposition of Ni-Fe<sub>2</sub>O<sub>3</sub> nanocomposite coating on steel, *Surf Coat Technol* 235: 691-698, 2013.
- [8] S.T. Aruna, C.N. Bindu, V. Ezhil Selvi, V.K. William Grips, K.S. Rajam, Synthesis and properties of electrodeposited Ni/ceria nanocomposite coatings, *Surf Coat Technol* 200 (24): 6871-6880, 2006.
- [9] Z. Geng, Y. Liu, H. Zhang: Tribological properties of electrodeposited Ni-ZrO<sub>2</sub> nanocomposite coatings on copperplate of crystallizer, *Surf Eng* 35 (10): 919-926, 2019.
- [10] I. Makarova, I. Dobryden, D. Kharitonov, A. Kasach, J. Ryl, E. Repo, E. Vuorinen: Nickel-nanodiamond coatings electrodeposited from tartrate electrolyte at ambient temperature, *Surf Coat Technol* 380: 125063, 2019.
- [11] J. Lapinski, D. Pletcher, F.C. Walsh: The electrodeposition of nickel-graphite composite layers, *Surf Coat Technol* 205 (21-22) : 5205-5209, 2011.
- [12] T.Borkar, S. Harimkar: Microstructure and wear behaviour of pulse electrodeposited Ni-CNT composite coatings, *Surf Eng* 27 (7): 524-530, 2011.
- [13] R. Zhang, G. Cui, X. Su, X. Yu, Z. Li: A novel functionally graded Ni-graphene coating and its corrosion resistance, *J Alloys Comp* 829: 154495, 2020.
- [14] A. Siddaiah, P. Kumar, A. Henderson, M. Misra, P.L.Menezes: Surface energy and tribology of electrodeposited Ni and Ni-graphene coatings on steel, *Lubricants*, 7 (10): 87, 2019.
- [15] L.D Xiang, Q. Shen, Y. Zhang, W. Bai, C. Nie: One-step electrodeposited Ni-graphene composite coating with excellent tribological properties, *Surf Coat Technol* 373: 38-46, 2019.
- [16] J. Wang, W. Lei, Y. Deng, Z. Xue, H. Qian, W. Liu, X. Li: Effect of current density on microstructure and corrosion resistance of Ni-graphene oxide composite coating electrodeposited under supercritical carbon dioxide, *Surf Coat Technol* 358: 765-774, 2019.
- [17] S. Singh, S. Samanta, A.K. Das, R.R. Sahoo: Tribological investigation of Ni-graphene oxide composite coating produced by pulsed electrodeposition, *Surf Interf* 12: 61-70, 2018.

- [18] G. Cieślak, M. Trzaska: Preparation and properties of nanocrystalline Ni/graphene composite coatings deposited by electrochemical method, *Pol J Chem Technol* 20 (1): 29-34, 2018.
- [19] N. Chronopoulou, D. Vozios, P. Schinas, E.A. Pavlatou: Electrodeposition and characterization of electroplated Ni/Graphene composite coatings, *Mater Today: Proceed* 5 (4): 27653-27661, 2018.
- [20] H.S.Maharana, P.K. Katiyar, K. Mondal: Structure dependent super-hydrophobic and corrosion resistant behavior of electrodeposited Ni-MoSe<sub>2</sub>-MWCNTcoating, *Appl Surf Sci* 478: 26-37, 2019.
- [21] A. Saini, B.S. Pabla, S.S.Dhami: Preparation and characterization of electrodeposited Ni-TiC, Ni-TiN, and Ni-TiC-TiN composite coatings on tungsten carbide cutting tool, *Proceed Inst Mechan Eng. Part J: Eng and Tribology*, 233: 1688, 2019.
- [22] P.F. Manicone, P. Rossi Iommetti, L. Raffaelli: An overview of zirconia ceramics: Basic properties and clinical applications, *J Denti* 35 (11):819-826, 2007.
- [23] Z. Peng, P. Shi, Y. Deng: Corrosion rate of Ni-ZrO<sub>2</sub> nano-coatings forecasted by GRNN, *ACM Int Conf. Proceed Series*, 236-241, 2020.
- [24] W. Ge, T. He, M. Wang, J. Li: Nano-grain Ni/ZrO<sub>2</sub> functional gradient coating fabricated by double pulses electrodeposition with enhanced high temperature corrosion performance, *Coatings*, 10 (4): 332, 2020.
- [25] A.K. Kasar, M.U. Bhutta, Z.A. Khan, P.L. Menezes: Corrosion performance of nanocomposite coatings in moist SO<sub>2</sub> environment, *Int J Advan Manuf Technol* 106 (11-12): 4769-4776, 2020.
- [26] B. Bostani, N. Parvini Ahmadi, S.Yazdani, R. Arghavanian: Synthesis and characterization of functionally gradient Ni-ZrO<sub>2</sub> composite coating, *Prot Met Phys Chem Surf*, 54 (2): 222-229, 2018.
- [27] B. Bostani, R. Arghavanian, N. Parvini Ahmadi, S. Yazdani: Fabrication and properties evaluation of functionally graded Ni-NCZ composite coating, *Surf Coat Technol* 328: 276-282, 2017.
- [28] Z. Geng, Y. Liu, H. Zhang: Tribological properties of electrodeposited Ni-ZrO<sub>2</sub> nanocomposite coatings on copperplate of crystallizer, *Surf Eng* 35 (10): 919-926, 2019.
- [29] S.T. Aruna, A.S. Mukasyan: Combustion synthesis and nanomaterials, *Curr Opin Solid State Mater Sci* 12 (3-4): 44-50, 2008.
- [30] S.T. Aruna, A. Kiran, M. Shilpa: Reclamation of thermal power plant waste as a distributed phase in electrodeposited Ni composite coating, *Surf Eng* 35 (12): 1042-1047, 2019.
- [31] S. Spanou, E.A. Pavlatou, N. Spyrellis: Ni/nano-TiO<sub>2</sub> composite electrodeposits: Textural and structural modifications, *Electrochim Acta*, 54: 2547-2555, 2009.
- [32] S.T. Aruna, V.K. William Grips, K.S. Rajam: Ni-based electrodeposited composite coating exhibiting improved microhardness, corrosion and wear resistance properties, *J Alloys Comp*, 468: 546-552, 2009.
- [33] M. Stern Geary: Electrochemical polarisation: A theoretical analysis of the shape of polarization curves, *J Electrochem Soc*, 104: 56-63, 1957.
- [34] R. Holm: *Electric Contacts*, Almquist and Wiksells, Stockholm, Section 40, 1946.
- [35] J.F. Archard: Contact and rubbing of flat surfaces, *J Appl Phys* 24: 981-988, 1953.
- [36] Y. Zhou, H. Zhang, B. Qian: Friction and wear properties of the co-deposited Ni-SiC nanocomposite coating, *Appl Surf Sci* 253(20): 8335-8339, 2007.
- [37] T. E. Fischer, P.A. Michael, S. Jahanmir: Influence of fracture toughness on the wear resistance of yttria-doped zirconium oxide, *J Amer Ceram Soc* 72(2): 252-257, 1989.